REFERENCES AND NOTES

1. S. E. Woosley and T. A. Weaver, *Annu. Rev. Astron. Astrophys.* **24**, 205 (1986).
2. The "A" designates it as the first supernova discovered in that year.
3. W. D. Arnett, J. N. Bahcall, R. P. Kirshner, S. E. Woosley, *Annu. Rev. Astron. Astrophys.* **27**, 629 (1989).
4. A. Burrows, J. Hayes, B. A. Fryxell, *Astrophys. J.* **450**, 830 (1995); H.-Th. Janka and E. Müller, *Astron. Astrophys.* **306**, 167 (1996); A. Mezzacappa *et al.*, *Astrophys. J.*, in press.
5. B. P. Schmidt *et al.*, *Astrophys. J.* **432**, 42 (1994); R. G. Eastman, B. P. Schmidt, R. P. Kirshner, *ibid.* **466**, 911 (1996).
6. C. J. Burrows *et al.*, *ibid.* **452**, 680 (1995).
7. P. Lundqvist and C. Fransson, *ibid.* **464**, 924 (1996).
8. R. M. West, A. Lauberts, H. E. Jorgensen, H. E. Schuster, *Astron. Astrophys.* **177**, L1 (1987).
9. J. M. Blondin and P. Lundqvist, *Astrophys. J.* **405**, 337 (1993); C. L. Martin and D. Arnett, *ibid.* **447**, 378 (1995).
10. P. Podsiadlowski, *Publ. Astron. Soc. Pac.* **104**, 717 (1992).
11. The term heavy elements refers to atomic species other than H and He.
12. L. Ball, D. Campbell-Wilson, D. F. Crawford, A. J. Turtle, *Astrophys. J.* **453**, 864 (1995).
13. B. Gaensler *et al.*, *ibid.* **479**, 845 (1997).
14. P. Duffy, L. Ball, J. G. Kirk, *ibid.* **447**, 364 (1995).
15. G. Hasinger, B. Aschenbach, J. Trümper, *Astron. Astrophys.* **312**, L9 (1996).
16. R. A. Chevalier and V. V. Dwarkadas, *Astrophys. J.* **452**, L45 (1995).
17. K. J. Borkowski, J. M. Blondin, R. McCray, *ibid.* **476**, L31 (1997).
18. The symbol N V denotes a line of four-times–ionized nitrogen (N I is neutral nitrogen). In this notation, a single bracket refers to a semiforbidden transition, and a double bracket, to a forbidden transition (rarely occurring on Earth).
19. D. Luo, R. McCray, J. Slavin, *Astrophys. J.* **430**, 264 (1994); K. J. Borkowski, J. M. Blondin, R. McCray, *ibid.* **477**, 281 (1997).
20. J. D. Kurfess, *ibid.* **399**, L137 (1992); D. D. Clayton, M. D. Leising, L.-S. The, W. N. Johnson, J. D. Kurfess, *ibid.*, p. L141.
21. F. X. Timmes, S. E. Woosley, D. H. Hartmann, R. D. Hoffman, *ibid.* **464**, 332 (1996).
22. N. N. Chugai, R. A. Chevalier, R. P. Kirshner, P. M. Challis, *ibid.*, in press.
23. C. Fransson and C. Kozma, *ibid.* **408**, L25 (1993); C. Kozma and C. Fransson, preprint (1997).
24. Filling factor refers to the fraction of the volume that is occupied by a particular kind of gas.
25. H. Li, R. McCray, R. A. Sunyaev, *Astrophys. J.* **419**, 824 (1993).
26. J. Spyromilio and P. A. Pinto, in *SN 1987A and Other Supernovae*, I. J. Danziger and K. Kjär, Eds. (European Southern Observatory, Garching, Germany, 1991), pp. 423–429.
27. M. R. Haas *et al.*, *Astrophys. J.* **360**, 257 (1990).
28. M. Herant and W. Benz, *ibid.* **387**, 294 (1992).
29. J. Pun and R. P. Kirshner, *Bull. Am. Astron. Soc.* **28**, 1330 (1996).
30. C. L. Fryer, in *SN 1987A: 10 Years Later*, M. M. Phillips and N. B Suntzeff, Eds. (Astronomical Society of the Pacific, San Francisco, in press).
31. R. A. Chevalier, *Astrophys. J.* **346**, 847 (1989); M. Colpi, S. L. Shapiro, I. Wasserman, *ibid.* **470**, 1075 (1996).
32. K. Nomoto *et al.*, *Nature* **364**, 507 (1993); P. Podsiadlowski, J. Hsu, P. C. Joss, R. R. Ross, *ibid.*, p. 509; S. E. Woosley, R. G. Eastman, T. A. Weaver, P. A. Pinto, *Astrophys. J.* **429**, 300 (1994).
33. T. Suzuki and K. Nomoto, *Astrophys. J.* **455**, 658 (1995); C. Fransson, P. Lundqvist, R. A. Chevalier, *ibid.* **461**, 993 (1996).
34. J. M. Marcaide *et al.*, *Science* **270**, 1475 (1995).
35. R. A. Chevalier and C. Fransson, *Astrophys. J.* **420**, 268 (1994).
36. A. V. Filippenko, T. Matheson, A. J. Barth, *Astron. J.* **108**, 2220 (1994).
37. B. Leibundgut, in *Circumstellar Media in the Late Stages of Stellar Evolution*, R. E. S. Clegg, I. R. Stevens, W. P. S. Meikle, Eds. (Cambridge Univ. Press, Cambridge, 1994), p. 100–111.

38. I thank the Supernova Intensive Study (SINS) collaboration (R. Kirshner, principle investigator) for their help with the HST data, P. Challis of that collaboration for figure preparation, and A. Filippenko for use of the Keck spectrum. C. Fransson and R. McCray made useful comments on the manuscript. My research on supernovae is supported in part by NSF grant AST-9314724. The SINS collaboration is supported by NASA through grant GO-2563.01-87A from the Space Telescope Science Institute, which is operated by the Association of Universities for Research in Astronomy under NASA contract NAS 5-26555.

Type Ia Supernovae: Their Origin and Possible Applications in Cosmology

Ken'ichi Nomoto,* Koichi Iwamoto, Nobuhiro Kishimoto

Spectroscopic and photometric evidence indicates that Type Ia supernovae (SNe Ia) are the thermonuclear explosions of accreting white dwarfs. However, the progenitor binary systems and hydrodynamical models for SNe Ia are still controversial. The relatively uniform light curves and spectral evolution of SNe Ia have led to their use as a standard candle for determining cosmological parameters, such as the Hubble constant, the density parameter, and the cosmological constant. Recent progress includes the calibration of the absolute maximum brightness of SNe Ia with the Hubble Space Telescope, the reduction of the dispersion in the Hubble diagram through the use of the relation between the light curve shape and the maximum brightness of SNe Ia, and the discovery of many SNe Ia with high red shifts.

Supernovae are classified spectroscopically as Type I if they have no hydrogen lines in their optical spectra and Type II if they have hydrogen lines in their optical spectra. Type I supernovae (SNe I) are further subclassified into types Ia, Ib, and Ic on the basis of spectra observed early in their explosion (early-time spectra) (*1*). SNe Ia are characterized by the presence of a deep Si II absorption line near wavelength 6150 Å (Fig. 1), and their late-time spectra are dominated by strong blends of Fe emission lines. SNe Ib and Ic, in contrast, do not show this Si line. Moderately strong He I lines, especially at 5876 Å, distinguish SNe Ib from SNe Ic in early-time spectra; that is, SNe Ib exhibit absorption lines of He I, whereas these lines are weak or absent in SNe Ic (*1*). SNe II, Ib, and Ic are now generally thought to result from the explosion of massive stars—SNe II from single stars and SNe Ib and Ic from binary stars. There are spectroscopic and photometric indications that SNe Ia originate from white dwarfs that are composed of C + O with strongly degenerate electrons and have accreted sufficient mass from a companion to trigger an explosion.

However, the progenitor systems and hydrodynamical models for SNe Ia are still controversial. Many issues need to be resolved, including (i) double-degenerate (DD) versus single-degenerate (SD) scenarios, that is, whether the companion of the white dwarf is also an electron-degenerate white dwarf or is a nondegenerate [main sequence (MS) or evolved red giant] star; (ii) Chandrasekhar mass (Ch) (*2*) versus sub–Chandrasekhar mass (sub-Ch) models; and (iii) the explosion mechanism in the Ch models. The answers to these questions could lead to improved understanding of the complicated evolution of close binaries as well as the physics of thermonuclear explosions (*3*). The relatively uniform light curves and spectral evolution of SNe Ia have led to their use as a standard candle to determine the Hubble constant (H_0), the density parameter (Ω_M), and the cosmological constant (Ω_Λ) (*4*). SNe Ia are important standard candles because they are bright enough to be observed out to a red shift (z) of $\sim$1. Variations of light curves and spectra among SNe Ia have recently received attention. SNe Ia with higher maximum brightnesses tend to show a slower decline in their light curves (*5, 6*) (Fig. 2). This review summarizes our current understanding of SNe Ia and focuses on these controversial issues.

Progenitors

White dwarfs composed of C + O are formed from intermediate mass stars ($M < 8\ M_\odot$, where $M_\odot$ is the mass of our sun), undergo cooling, and eventually become

The authors are in the Department of Astronomy, University of Tokyo, Bunkyo-ku, Tokyo 113, Japan.

*To whom correspondence should be addressed.

dark matter as they evolve toward fainter luminosities. In a close binary system, the white dwarf evolves differently because the companion star expands to transfer matter to the white dwarf; the accreting white dwarfs are rejuvenated and, in certain cases, undergo thermonuclear explosions to give rise to SNe Ia. Theoretically, the Ch white dwarf models and the sub-Ch models have been considered to explain the origin of SNe Ia (*7*). Various evolutionary scenarios have been proposed, including (i) merging of double C + O white dwarfs with a combined mass exceeding the Ch limit (a DD scenario) (*8*) and (ii) accretion of H or He by mass transfer from a binary companion at a relatively high rate (an SD scenario) (*7, 9*).

The DD-Ch scenario is favored from the theoretical estimate of frequencies of the occurrence of SNe Ia. This has stimulated a search for DD systems, but few such systems have been discovered, and their combined mass is smaller than Ch (*7*). For an SD scenario, the accreting white dwarf undergoes H burning near the surface, which increases or decreases the white dwarf mass, depending mainly on the accretion rate, $\dot{M}$ (*9*). Ch white dwarfs can be formed with a relatively high accretion rate such as $\dot{M} \approx 10^{-8}$ to 10^{-6} $M_\odot$ year^{-1} because of relatively small mass ejection after H or He shell burning. Recently, it was found that this range of $\dot{M}$ can be extended to a rate faster than 10^{-6} $M_\odot$ year^{-1} (*10*). With such a high rate, the white dwarf undergoes wind mass loss without expanding its radius, thereby increasing its mass by steady H burning. The SD–sub-Ch scenario—that is, the explosion of sub-Ch white dwarfs—is a possible outcome of accretion with 4×10^{-8} $M_\odot$ year$^{-1} \gtrsim \dot{M} \gtrsim 10^{-9}$ $M_\odot$ year^{-1}. In this case, the ignited He shell flash is strong enough to initiate an off-center He detonation (*11, 12*), which induces various types of explosions.

Promising candidates for the white dwarf's companion stars for the SD scenario are (i) stars with MS masses of 1 to 1.5 $M_\odot$, which fill the Roche lobe when they evolve through red giants, and (ii) the 2 to 3 $M_\odot$ stars, which undergo mass transfer near the MS. These cases of relatively fast accretion onto the white dwarf can correspond to supersoft x-ray sources (*13*), symbiotic stars (*7*), or both.

To discriminate among the SD–sub-Ch, SD-Ch, and DD-Ch scenarios, we used photometric and spectroscopic diagnostics. If any H or He were detected, the DD model could be ruled out. Although high-velocity H has not been observed in any SNe Ia, the upper limit to the H abundance ($\sim 10^{-4}$ $M_\odot$) is still too high to rule out the SD models. The H-rich materials in the companion star may be engulfed in the exploding material; thus, the detection of low-velocity H could be critical (*14*).

Explosion Models

Once explosive nuclear burning is ignited, it induces thermonuclear explosion of the white dwarf. The outcome of this explosion depends on how the nuclear flames and shock waves propagate for the Ch and sub-Ch white dwarfs. The physics involved in these processes is rather complex, and multidimensional simulations have been conducted to understand these processes (*15*). The results are still preliminary, and so we focus here on those models that can account for the basic features of SNe Ia, namely, an explosion energy of $\sim 10^{44}$ J, the synthesis of a large amount of ^{56}Ni (0.4 to 1 $M_\odot$), and the production of a substantial amount of intermediate-mass elements at expansion velocities of $\sim$10,000 km s^{-1} near the maximum brightness of the SN explosion.

Chandrasekhar mass models. Carbon is ignited in the central region of the white dwarf when the central density exceeds $\sim 10^9$ g cm^{-3}. Because of strong electron degeneracy, C burning is so explosive that it incinerates the material into Fe-peak elements (*16*). Afterward, the explosive nuclear flame propagates outward. The flame front is subject to various types of instabilities, including thermal instabilities, the Landau-Darrius instability, the Rayleigh-Taylor instability, and the Kelvin-Helmholtz instability (*17*). The flame speed depends on the development of these instabilities and the resulting turbulence, requiring further extensive simulations on large and small scales as well as suitable modeling of the turbulence. Behind the flame front, materials undergo explosive nuclear burning of Si, O, Ne, and C. The nucleosynthesis products depend mainly on peak temperatures, which in turn depend on the densities encountered by the flame. For densities from 10^{10} to 10^6 g cm^{-3}, the products range from Fe-peak elements (mostly ^{56}Ni) to intermediate-mass elements (Ca, Ar, S, and Si), O-Ne-Mg, and C + O.

During the subsonic propagation of the deflagration wave, the densities of the whole white dwarf are decreasing because of expansion. Therefore, the densities encountered by the flame are determined by its speed, which is still uncertain. Several plausible models have been presented with one-dimensional codes (*11, 12*). In carbon deflagration models, such as model W7 (*18*), the average flame speed is as high as one-fifth of the sound speed. A sequence of nucleosynthesis reactions produces ^{56}Ni, Ca-S-Si, O-Ne-Mg, and C + O behind the deflagration wave. Because of fast propagation of the flame, the transition to the detonation could be induced by shock compression in the outer low-density layers, which would produce some variations of ^{56}Ni mass and distribution, as seen in pecu-

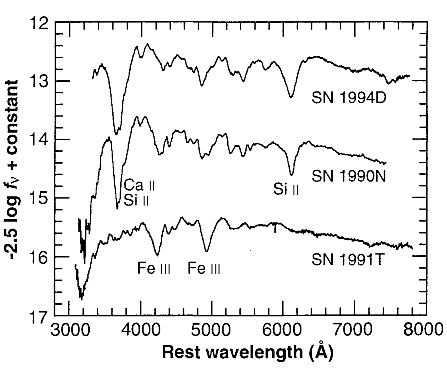

Fig. 1. Spectra of SNe Ia (SN 1994D and SN 1990N) about 1 week before maximum brightness (the flux f_ν is in units of ergs s^{-1} cm^{-2} Hz^{-1}). SN 1991T was peculiar (*1*).

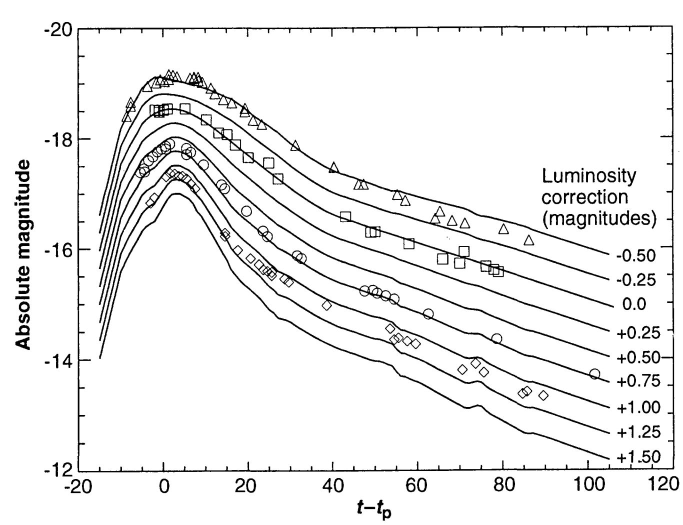

Fig. 2. Empirical family of the visual light curves of SNe Ia, which shows the brightness–decline rate relation. The triangles, squares, circles, and diamonds denote SNe 1991T, 1981B, 1986G, and 1991bg, respectively (*6*).

liar SNe Ia such as SN 1991T (Fig. 1). In contrast, delayed detonation models assume that the early propagation of the deflagration is as slow as a few percent of the sound speed, producing ~0.1 $M_\odot$ of ^{56}Ni, and hence the transition from deflagration to detonation could occur at densities of 1×10^7 to 3×10^7 g cm^{-3}. In this case, the bulk of the white dwarf has expanded to lower densities, so that the detonation wave synthesizes Fe-peak elements and intermediate-mass elements (*19*). In the pulsating delayed detonation model, the transition to detonation is assumed to occur near the maximum compression (*20*). Possible variations of the transition density could produce variations of the ^{56}Ni mass produced.

Sub-Chandrasekhar mass models. A central C detonation can be initiated by a He detonation–induced shock wave (*12, 21*). Merging of double white dwarfs could ignite a central C detonation (*22*). If the white dwarf mass is less than 1.07 $M_\odot$, the densities of the white dwarf matter encountered by the detonation wave can be suitable to produce sufficient amounts of ^{56}Ni and Si-Ca-O. Variations of the white dwarf mass could cause the variations of the light curves of the resultant SN Ia.

Constraints on still uncertain parameters in these models, such as the central ignition density, the flame speed, and the deflagration-detonation transition density, can be provided by comparisons of theoretical spectra and light curves with observations and by comparisons of nucleosynthesis consequences with solar isotopic ratios. A combination of processes from various models may be responsible for the variations in characteristics of the observed SNe Ia.

Spectra and Light Curves

Spectra. Spectra of SNe Ia are generally homogeneous but show some important variations. Because SNe Ia do not have a thick H-rich envelope, elements newly synthesized during the explosion can be observed in the spectra. Thus, comparison between the synthetic spectra and observations is a powerful diagnostic of the dynamics and nucleosynthesis suggested by the models. Non–local thermodynamical equilibrium (LTE) spectra have been calculated and can be used to compare with observations. A typical example (Fig. 3) shows agreement between the C deflagration model (unmixed W7) and the observed optical spectra of SNe 1992A and 1994D (*23*). The material velocity at the stellar surface near maximum brightness is ~10,000 km s^{-1} and the spectral features are identified as those of Fe, Ca, S, Si, Mg, and O. This implies that the abundance distribution in the velocity space may be similar to W7. The synthetic spectra for the sub-Ch models seem to be less satisfactory (*23, 24*).

Regarding the heterogeneity in the spectra, SNe 1991T (Fig. 1) and 1991bg are the two extreme examples that have revealed the presence of spectroscopically peculiar SNe Ia (*25*). The pre–maximum brightness spectra of SNe Ia show a significant variation of the composition and expansion velocities of the outermost layers, whereas the postmaximum spectra are relatively uniform except for SN 1991bg. The different ^{56}Ni mass may produce the variation of the spectra (*26*). Further analysis could provide the abundance distribution of various elements (Fe, Ca, Si, Mg, O, C, and others) in velocity space (*27*).

Light curves. Recent high-quality charge-coupled device (CCD) observations of SNe Ia have, on one hand, supported the basic homogeneity of the optical light curve shape of SNe Ia. Good examples include SNe 1980N and 1981D in the galaxy NGC 1316, whose light curve shapes and brightnesses were almost identical. On the other hand, the observations have established significant variations of the maximum brightness, the light curve shape, and their correlation (Fig. 2). In theoretical models, the explosion energy goes into the kinetic energy of expansion, *E*. The light curves are powered by the radioactive decay sequence $^{56}\text{Ni} \rightarrow {}^{56}\text{Co} \rightarrow {}^{56}\text{Fe}$. The calculated light curve reaches its peak at about 15 to 20 days after the explosion and declines because of the increasing transparency of the ejecta to gamma rays as well as the decreasing input of radioactivity. The light curve shape depends mainly on the effective diffusion time $\tau_m \propto (\kappa M/v_{\rm exp}c)^{1/2}$, where κ is opacity, *c* is the speed of light, and $v_{\rm exp} \propto (E/M)^{1/2}$ (*15*). For longer τ_m, the decline of the light curve is slower. For larger $M_{\rm Ni}$, the brightness is higher. For the Ch models, typical values of $M_{\rm Ni}$ and *E* are similar to those of W7, that is, $M_{\rm Ni} = 0.6 \pm 0.1\ M_\odot$ and $E = 1.3 \pm 0.1 \times 10^{44}$ J.

The observed uniformity in the light curve implies a uniformity of *M*, *E*, and $M_{\rm Ni}$. A homogeneous *M* and *E* can be naturally accounted for with the Ch models, although the central density can vary with a small difference of mass near the Ch limit. For the sub-Ch models, the accretion process must somehow choose a relatively narrow mass range, such as $M \approx 1.0$ to 1.1 $M_\odot$. The reported variation of the maximum brightness of SNe Ia (*5, 6*) may be a result of the variations of the ^{56}Ni mass. The amount of ^{56}Ni depends on (i) the flame speed in the fast-deflagration models, (ii) the location and density of the transition to a detonation in the delayed or late-detonation models, and (iii) the white dwarf mass in the sub-Ch models. Because of variations of these parameters, variation of the ^{56}Ni mass may be possible. For the Ch models, the dependence of optical opacities on the temperature is important (*28*). A smaller mass of ^{56}Ni means less heating of the surface layer, thus lowering κ and τ_m. This effect might explain the relation between brightness and the decline rate of the light curve. For the sub-Ch models, $M_{\rm Ni}$ varies approximately in proportion to *M*. Then, for larger *M*, $M_{\rm Ni}$ is larger and τ_m is longer; in other words, brighter SNe Ia tend to decline more slowly (*15*).

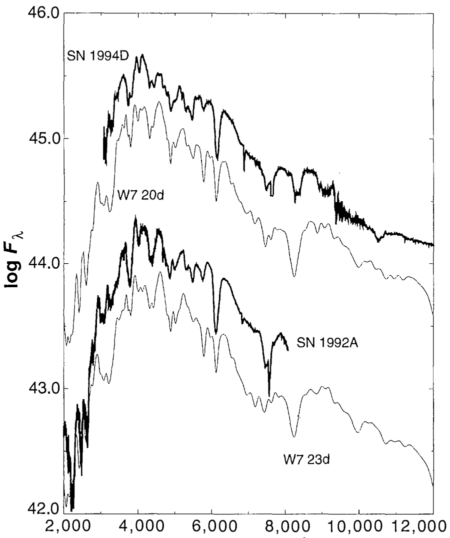

Fig. 3. The non-LTE spectra of carbon deflagration model W7 (unmixed) at 20 and 23 days after explosion, which are compared with SNe 1992A and 1994D, respectively (*23*). The flux F_λ is in units of ergs s^{-1} Å^{-1}.

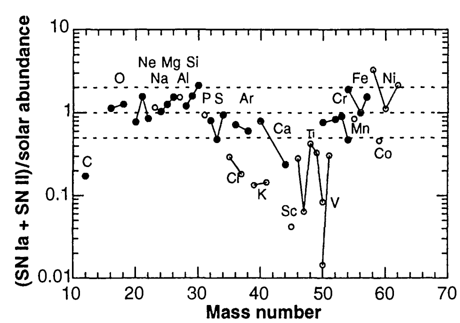

Fig. 4. Solar abundance pattern based on synthesized heavy elements from a composite of SNe Ia and SNe II with the most probable ratio (*30*). Open and solid circles are used to clarify correspondence between data points and elements. Dashed lines indicate typical uncertainties of a factor of 2 involved in the observational and theoretical abundances, where the abundance ratios are normalized to unity for ^{56}Fe.

Role of Nucleosynthesis in Galactic Chemical Evolution

Supernovae of different types have different progenitors, thus producing different heavy elements on different time scales during the chemical evolution of galaxies. A reasonable mixture of the heavy element yields from SNe Ia and SNe II should be able to explain the solar abundance pattern of heavy elements from O to the Fe group. Nucleosynthesis products of SNe Ia and SNe II can be combined with various ratios and compared with solar abundances of heavy elements and their isotopes. If the nucleosynthesis products of SNe II as a function of stellar masses (*29*) are adopted with an upper mass limit of 50 $M_\odot$ and the nucleosynthesis products of SNe Ia are those from model W7, the best fit to known solar abundances is obtained if the number of SNe Ia that have occurred relative to SNe II is $N_{Ia}/N_{II} = 0.12$ (*30*) (Fig. 4). This is consistent with observation-based estimates that the SNe Ia frequency is as low as 10% of total supernova occurrence (*31*).

With this relative frequency, ^{56}Fe from SNe Ia is about 50% of total ^{56}Fe from all SNe. For the Ch models, the abundance ratios between neutron-rich species and ^{56}Fe provide an important constraint on the progenitor system. The central density of the white dwarf at thermonuclear runaway must be as low as $\lesssim 2 \times 10^9$ g cm^{-3} to avoid overabundances of ^{58}Ni, ^{54}Cr, and ^{50}Ti relative to ^{56}Fe, although the exact density depends on the flame speed (*30*). Such a low central density can be realized by accretion as fast as $\dot{M} > 1 \times 10^{-7}$ $M_\odot$ year^{-1}, which is consistent with the SD-Ch scenario. SNe Ia yields thus contribute Fe enrichment to the chemical evolution of the galaxies. Because the progenitors of SNe Ia are low-mass stars with relatively long lifetimes, Fe could be used as a clock to look back into the timing of galaxy formation (*32*).

Cosmological Parameters

Hubble constant. SNe Ia are very good, but not perfect, standard candles. The accuracy of the determination of H_0 using SNe Ia depends on (i) whether the peak absolute-magnitude dispersion of SNe Ia is sufficiently small, and (ii) whether a precise absolute-magnitude calibration of a SN Ia can be made. Recent progress has been made in the empirical determination of H_0. For the dispersion, the correlation between the maximum brightness and the decline rate (or the light curve shape) is taken into account. Multicolor light curve shapes are also used for further corrections (6). This reduces the dispersion from 0.4 to 0.2 magnitudes in the Hubble diagram for SNe Ia (*6*, *33*) (Fig. 5). For the calibration, the distances to several host galaxies of SNe Ia (SNe 1895B, 1937C, 1960F, 1972E, 1981B, 1989B, and 1990N) have been determined from Hubble Space Telescope observations of Cepheids in these galaxies (*34*). On the basis of these data, H_0 is estimated to be 58^{+7}_{-8} (*34*), 63.1 ± 6.3 (*33*), 64 ± 6 (*6*), and 55 ± 3 (*35*) km s^{-1} Mpc^{-1}.

Successful theoretical models can, in principle, give the absolute maximum luminosities, thus providing good estimates of H_0 and Ω_M. The maximum luminosity L_{max} of SNe Ia when explained with radioactive decay models has been used to estimate H_0 (*36*). From a comparison with individual SNe Ia, $H_0 = 67 \pm 9$ km s^{-1} Mpc^{-1} (*24*) and 59 ± 13 km s^{-1} Mpc^{-1} (*37*). In addition, a fit of the late-time synthetic spectra to observations gave $H_0 = 68 \pm 13$ km s^{-1} Mpc^{-1} (*38*).

These estimated values tend to converge to $H_0 \approx 58$ to 65 km s^{-1} Mpc^{-1} where the error bars overlap. The higher H_0 is in conflict with the age of the universe for $\Omega_M = 1$ and $\Omega_\Lambda = 0$, whereas the lower H_0 could avoid this problem. Further efforts to reduce the error bars will require the reexamination of sampling, extinction corrections, and so on.

Density parameter. In determining Ω_M and Ω_Λ from SNe Ia, absolute calibration of the distances to SNe Ia is not needed, but more accurate measurements of magnitudes and z values are necessary. In addition to the dispersion problem, whether a significant value of Ω_M can be obtained depends on (i) whether a suitable sample of remote SNe Ia can be obtained, and (ii) whether the peak luminosities of SNe Ia are sufficiently free from the effects of cosmic and galactic chemical evolutions.

More than 60 SNe Ia with high z values have been observed (*39*, *40*) (Fig. 5). Values derived from the first seven SNe at $z > 0.35$ are $\Omega_M = 0.88^{+0.69}_{-0.60}$ for $\Omega_\Lambda = 0$ or $\Omega_M = 1 - \Omega_\Lambda = 0.94^{+0.34}_{-0.28}$ for $\Omega_M + \Omega_\Lambda = 1$, assuming that evolutionary effects are small. To clarify whether the nature of high z SNe Ia is the same as that of nearby SNe Ia, it is important to identify the progenitors' evolution and population (*41*). Systematic studies on the effects of metallicity of the progenitors are under way.

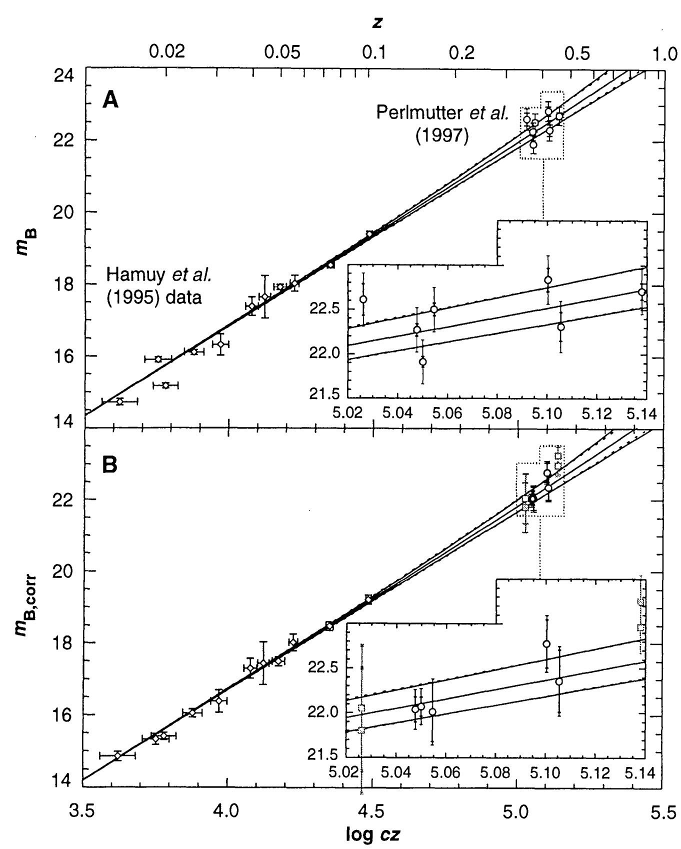

Fig. 5. Hubble diagram for the seven high z SNe Ia out to $z = \sim 0.6$, with some of the low z SNe (*33*): (**A**) uncorrected blue magnitudes m_B, and (**B**) m_B with corrections of the brightness–decline rate relation (*39*). The solid curves are theoretical m_B values for (Ω_M, Ω_Λ) = (0,0) (top curve), (1,0) (middle curve), and (2,0) (bottom curve). The square data points in (B) are not used in the analysis because these points are corrected on the basis of the extrapolation outside the range of light curve widths of low z SNe.

REFERENCES AND NOTES

1. A. V. Filippenko, *Annu. Rev. Astron. Astrophys.*, in press; D. Branch, K. Nomoto, A. V. Filippenko, *Comments Astrophys.* **15**, 221 (1991).
2. Ch is the maximum mass limit of the white dwarfs in hydrostatic equilibrium, with a typical value of 1.46 $M_\odot$. For larger masses, pressures exerted by degenerate electrons cannot sustain the gravity because of the special relativistic effect.
3. *Thermonuclear Supernovae*, P. Ruiz-Lapuente, R. Canal, J. Isern, Eds. (Kluwer, Dordrecht, Netherlands, 1997); this book includes most of the recent progress in SNe Ia.

4. D. Branch and G. Tammann, *Annu. Rev. Astron. Astrophys.* **30**, 359 (1992).
5. M. M. Phillips, *Astrophys. J.* **413**, L105 (1993).
6. A. G. Riess, W. N. Press, R. P. Kirshner, *ibid.* **438**, L17 (1995); *ibid.* **473**, 88 (1996).
7. D. Branch, M. Livio, L. R. Yungelson, F. R. Boffi, E. Baron, *Publ. Astron. Soc. Pac.* **107**, 717 (1995); A. Renzini, in *IAU Colloquium 145, Supernovae and Supernova Remnants,* R. McCray and Z. Wang, Eds. (Cambridge Univ. Press, Cambridge, 1996), pp. 77–85.
8. I. Iben Jr. and A. Tutukov, *Astrophys. J. Suppl. Ser.* **55**, 335 (1984); R. Webbink, *Astrophys. J.* **277**, 355 (1984).
9. For example, K. Nomoto, *Astrophys. J.* **253**, 798 (1982); ——— and Y. Kondo, *ibid.* **367**, L19 (1991); K. Nomoto *et al.*, in *Supernovae* (Les Houches, Session LIV), S. Bludman *et al.,* Eds. (Elsevier Science, Amsterdam, 1994), pp. 199–249.
10. I. Hachisu, M. Kato, K. Nomoto, *Astrophys. J.* **470**, L97 (1996).
11. K. Nomoto, *ibid.* **257**, 780 (1982); M. Hashimoto, K. Nomoto, K. Arai, K. Kaminisi, *ibid.* **307**, 687 (1986).
12. S. E. Woosley and T. A. Weaver, *ibid.* **423**, 371 (1994).
13. E. P. J. van den Heuvel, D. Bhattacharya, K. Nomoto, S. A. Rappaport, *Astron. Astrophys.* **262**, 97 (1992); S. A. Rappaport, R. DiStefano, J. Smith, *Astrophys. J.* **426**, 692 (1994).
14. P. Ruiz-Lapuente *et al.*, *Nature* **365**, 728 (1993).
15. W. D. Arnett, *Nucleosynthesis and Supernovae* (Princeton Univ. Press, Princeton, NJ, 1996); S. E. Woosley, in *Supernovae*, A. Petschek, Ed. (Springer, New York, 1990), pp. 182–212.
16. Fe peak elements consist of mostly Fe and Ni with some Ti, V, Cr, Mn, and Co.
17. For example, J. Niemeyer and W. Hillebrandt, *Astrophys. J.* **452**, 769 (1995); J. Niemeyer and S. E. Woosley, *ibid.* **475**, 740 (1997).
18. K. Nomoto, F.-K. Thielemann, K. Yokoi, *ibid.* **286**, 644 (1984); F.-K. Thielemann, K. Nomoto, K. Yokoi, *Astron. Astrophys.* **158**, 17 (1986); H. Yamaoka, T. Shigeyama, K. Nomoto, F.-K. Thielemann, *Astrophys. J.* **393**, L55 (1992).
19. A. M. Khokhlov, *Astron. Astrophys.* **245**, 114 (1991); S. E. Woosley and T. A. Weaver, in *Supernovae* (Les Houches, Session LIV), S. Bludman *et al.*, Eds. (Elsevier Science, Amsterdam, 1994), pp. 63–154.
20. A. M. Khokhlov, *Astron. Astrophys.* **245**, L25 (1991); W. D. Arnett and E. Livne, *Astrophys. J.* **427**, 314 (1994).
21. E. Livne, *Astrophys. J.* **354**, L53 (1990).
22. T. Shigeyama, K. Nomoto, H. Yamaoka, F.-K. Thielemann, *ibid.* **386**, L13 (1992); J. C. Wheeler and R. Harkness, *Rep. Prog. Phys.* **53**, 1467 (1990).
23. P. Nugent, E. Baron, D. Branch, A. Fisher, P. Hauschildt, *Astrophys. J.*, in press.
24. P. Höflich and A. Khokhlov, *ibid.* **457**, 500 (1996).
25. For example, P. Mazzali, I. J. Danziger, M. Turatto, *Astron. Astrophys.* **297**, 509 (1995); M. Turatto *et al.*, *Mon. Not. R. Astron. Soc.* **283**, 1 (1997).
26. P. Nugent, E. Baron, D. Branch, *Astrophys. J.* **455**, L147 (1995).
27. For example, D. Jeffery *et al.*, *ibid.* **397**, 304 (1992); A. Fisher, D. Branch, P. Hoflich, A. Khokhlov, *ibid.* **447**, L73 (1995); W. P. S. Meikle *et al.*, *Mon. Not. R. Astron. Soc.* **281**, 263 (1996).
28. P. Höflich *et al.*, *Astrophys. J.* **472**, L81 (1996).
29. M. Hashimoto, K. Nomoto, F.-K. Thielemann, *Astron. Astrophys.* **210**, L5 (1989); F.-K. Thielemann, K. Nomoto, M. Hashimoto, *Astrophys. J.* **460**, 408 (1996); T. Tsujimoto *et al.*, *Mon. Not. R. Astron. Soc.* **277**, 945 (1995); see also S. E. Woosley and T. A. Weaver, *Astrophys. J. Suppl. Ser.* **101**, 181 (1995).
30. K. Nomoto *et al.*, in (*3*), pp. 349–378.
31. S. van den Bergh and G. A. Tammann, *Annu. Rev. Astron. Astrophys.* **29**, 363 (1991).
32. For example, Y. Yoshii, T. Tsujimoto, K. Nomoto, *Astrophys. J.* **462**, 266 (1996).
33. M. Hamuy *et al.*, *Astron. J.* **109**, 1 (1995); *ibid.* **112**, 2398 (1996).
34. A. Sandage *et al.*, *Astrophys. J.* **460**, L15 (1996); A. Saha *et al.*, *ibid.*, in press.
35. B. E. Schaefer, *ibid.* **460**, L19 (1996).
36. W. D. Arnett, D. Branch, J. C. Wheeler, *Nature* **314**, 337 (1985).
37. D. Branch, P. Nugent, A. Fisher, in (*3*), pp. 715–734.
38. P. Ruiz-Lapuente, *Astrophys. J.* **465**, L83 (1996).
39. The Supernova Cosmology Project: S. Perlmutter *et al.*, *ibid.*, in press; *IAU Circular 6596* (1997).
40. The High-Z Supernova Search Team: B. Schmidt *et al.*, *IAU Circular 6602* (1997).
41. P. Ruiz-Lapuente, A. Burkert, R. Canal, *Astrophys. J.* **447**, L69 (1995); R. Canal, P. Ruiz-Lapuente, A. Burkert, *ibid.* **456**, L101 (1996).
42. Supported in part by a grant-in-aid for scientific research (05242102, 06233101, 4227) and COE research (07CE2002) of the Ministry of Education, Science, and Culture of Japan.

Planetary Nebulae: Understanding the Physical and Chemical Evolution of Dying Stars

Ronald Weinberger and Florian Kerber

Planetary nebulae are one of the few classes of celestial objects that are active in every part of the electromagnetic spectrum. These fluorescing and often dusty expanding gaseous envelopes were recently found to be quite complex in their dynamics and morphology, but refined theoretical models can account for these discoveries. Great progress was also made in understanding the mechanisms that shape the nebulae and the spectra of their central stars. In addition, applications for planetary nebulae have been worked out; for example, they have been used as standard candles for long-range distances and as tracers of the enigmatic dark matter.

Planetary nebulae (PNe) were so called because their often faint disks resembled images of Uranus and Neptune. The oldest known discovery of a PN dates back to Messier, who in 1784 catalogued the Dumbbell nebula, NGC 6853, as Messier 27 (*1*). Actually, PNe are gaseous nebulae, although they often contain a great deal of dust, and originate as envelopes thrown off from stars in advanced evolutionary stages. Starting as dense, compact objects, they brighten as they expand and fluoresce with radiation absorbed in the ultraviolet (UV) spectral range as the condensed core of the dying star attains a high surface temperature ($\geq$30,000 K) and radiates copiously at wavelengths less than 91.2 nm. Eventually, as the density of the expanding envelope drops, the surface brightness falls abruptly, and the nebulae disappear. The ejected material returns to the interstellar medium (ISM). The remnant stars, called central stars (CSs) because of their location in or near the centers of the PNe, become white dwarf stars during the latest phases of the evolution of the nebulae.

Planetary nebulae are found not only in our galaxy, but also in other galaxies. About one to two times every year, a star of mass $\leq$ 1 solar mass ($M_\odot$) is born in our Milky Way. Almost 99% of all stars are less massive than 10 $M_\odot$, and those with masses of 1 to 8 $M_\odot$ will almost certainly go through the PN phase, provided they are single stars or are in a wide binary (*2*). On the other hand, it has long been established that white dwarfs have a narrow range of masses sharply peaking around 0.6 $M_\odot$ (*3*). Consequently, in several cases, considerable mass is lost to the ISM, and a part of this mass, up to 1 $M_\odot$ per PN, is in the form of these nebulae, which usually expand with velocities of about 20 to 30 km s^{-1}.

The authors are at the Institut für Astronomie der Universität Innsbruck, Technikerstrasse 25/8, A-6020 Innsbruck, Austria.

Study of PNe and their CSs provides understanding about the chemical and physical evolution of the majority of stars. By comparing observations with theoretical models of star evolution, it was possible to understand why and how PNe form, how the nebulae and the CSs develop, and how the internal structure and chemical composition of the CS are reflected in the physical conditions of the PN (*4*). Astronomers also study PNe to learn about the chemical evolution of galaxies. The abundances of various elements in PNe trace the abundances of the ISM, from which the progenitor stars originally formed, and the surface abundances of the immediate precursor stars of PNe, which were enriched by material dredged up to their surfaces from interior regions of nucleosynthesis. Thus, by studying chemical abundances in PNe, astronomers are able to trace the history of galactic chemical evolution and help constrain models of stellar evolution. The abundances of the elements N, C, and He are the result of stellar nucleosynthesis, whereas O, Ne, Ar, and S trace the metallicity of the region in which the star formed (*5*).

Planetary nebulae are also useful yard-